Scanning tunnelling spectroscopy of unoccupied surface resonances at free-electron-like metal surfaces

1995 J. Phys.: Condens. Matter 7 2697

(http://iopscience.iop.org/0953-8984/7/14/010)

J. Phys.: Condens. Matter 7 (1995) 2697–2716. Printed in the UK

Scanning tunnelling spectroscopy of unoccupied surface resonances at free-electron-like metal surfaces

T Fondén†, S Papadia‡ and M Persson§

Department of Applied Physics, Chalmers University of Technology, S-412 96 Göteborg, Sweden

Received 23 August 1994, in final form 16 January 1995

Abstract. We extend and detail a previously developed model for formation of electronic resonances at free-electron-like metal surfaces, in order to calculate scanning tunnelling (ST) spectra. The effect of the tip is mimicked by inclusion of an external field, self-consistently, in a jellium description of the surface potential. The lattice-induced corrugation of the potential is included perturbatively via a pseudopotential. We compare our calculated ST spectra for Al(111) with experimental spectra for that surface and conclude that a peak occurring below the metal vacuum level is a 'crystal-derived' resonance, in the sense that lattice effects are crucial for its manifestation.

1. Introduction

The investigation of unoccupied electron states at surfaces is crucial for our understanding of phenomena taking place at surfaces, such as scattering of electrons, atoms and ions [1, 2, 3, 4] and vacuum tunnelling [5, 6, 7, 8]. A particular type of such a state is the image potential-induced series, produced when an electron is trapped in a potential well defined by the image potential part of the surface barrier on the vacuum side, and a projected band gap on the crystal side [9]. Experimentally, image potential states have been studied mainly by low-energy electron diffraction (LEED) and inverse photoemission spectroscopy (IPE) [10, 11, 12] and preferably at surfaces where a projected band gap exists at or close to the energy of the series. Theoretically, the existence of a high substrate reflectivity, as e.g. given by the presence of a band gap, has been crucial for the building up of an image state as described in multiple-scattering models [1, 2]. At energy ranges outside a metal band gap, the image states broaden into resonances and eventually cease to be resolvable by experimental means.

There are though experimental evidence and theoretical support that resonances persist at energies surprisingly far from band gaps. IPE spectra [12] of Al(111), where no projected band gaps exist in the probed region, revealed a spectral feature close to the vacuum level which was suggested to be an image resonance. Several authors provided calculations in favour of that explanation [13, 14, 15] with different viewpoints. The interpretation of IPE features close to the vacuum level in terms of the surface density of states (SDOS) was subsequently questioned by Schaich and Lee [16] who interpreted the spectral features

† Present address: Institute of Physics, 142 Riia Street, EE-2400 Tartu, Estonia.

‡ Present address: DSM/DRECAM/SRSIM, Centre d'Etudes de Saclay, F-91191 Gif sur Yvette, France.

§ To whom correspondence should be addressed. Electronic address: tfymp@fy.chalmers.se.

0953-8984/95/142697+20$19.50

as due to a matrix element effect, with no direct coupling to the SDOS of the metal. The calculations by Schaich and Lee [16] motivated further complementary studies of the unoccupied electronic states of free-electron-like metals.

The scanning tunnelling spectroscopy (STS) technique has been suggested as a possibility of obtaining information about the surface electronic structure [17, 18, 19, 20]. This spectroscopy has been proven to be able to give information for surface states on graphite [19] and Si [20]. It has also been asserted that STS provides identification of the image state spectrum on metals [5, 21]. In such experiments, the normalized conductance is recorded, often in a constant-current mode where the bias is varied under the condition of keeping the tunnel current constant. These curves are then related to the electronic states of the substrate within different theories.

We will in the following present a model for interpretation of conductance curves, which is an extension of the model in [14], and we demonstrate how peaks in the STS curves are connected to SDOS features of the substrate. Application of the model to Al(111) and comparison between STS and theoretical calculations demonstrate several resonances in the SDOS. In particular, we show that there is *one* resonance, below the metal vacuum level, which shows up in STS because of lattice effects—it is a 'crystal-derived' resonance. In this paper, we also correct an error in the evaluated phase shift within our model, made in our previous analysis [14, 22]. The basic conclusions are still valid but the calculated resonance positions are lowered in energy. Finally, the crystal reflectivities obtained in our model and in a two-band model [15] are compared and it is found that the two-band model underestimates the crystal reflectivity at energies far from the considered band gap.

The paper is organized as follows. In section 2, we present the different steps in our model. First, the construction of the potential between tip and substrate in the tunnelling geometry is described in subsection 2.1; the effects of the scattering from the ion core lattice are included in the expressions for the current density and in the expression for the substrate density of states, described in subsections 2.3 and 2.4, respectively. We present and discuss our results in section 3 by first comparing our calculated conductance curves with our calculated SDOS, obtained for different initial conditions in experiments; then we compare the calculated conductance to experimental conductance curves for Al(111). A summary is given in section 4. In the appendix, we present the detailed derivation of the crystal reflectivity and a comparison is made to the reflectivity obtained in a two-band model.

2. Model

Our calculations are based on a quasi-one-dimensional model where the starting point for the modelling of both the sample and the tip is the jellium model for a metal surface. This is motivated by the use of rather blunt tips in STS experiments. The calculated current densities in such a one-dimensional model should thus give a fair description of the actual experimental situation. In the following, we describe our model for the tip–sample interface potential and the calculation of the reflectivity from the sample crystal potential in detail. In addition we show how the tunnelling current and the surface-induced DOS are calculated using the obtained interface potential and crystal reflectivity. If not explicitly stated otherwise, Hartree atomic units are used throughout where $\hbar = m = e = 1$ (m is the electron mass).

2.1. Potential construction

We model the interface potential for the scanning tunnelling experiment on Al(111) for large initial separations between the tip and sample of typically 15–25 Å. In this situation, we expect to have a linear region in the interface potential for a constant external electric field F. The interface potential, $V_i(z)$, may then be decomposed into a tip and a sample part which are treated separately. This decomposition is not justified at short distances, e.g., below 5 Å where the barrier does not have a linear part, as can be seen in the work by Lang [23]. The potentials, $V_t(z)$ and $V_s(z)$, of the isolated tip and sample, respectively, are both modelled by the potential $V_0(z; \pm F_{ext})$ of a semi-infinite jellium ($z \to -\infty$ in the bulk) in external uniform electric fields $\pm F_{ext}$, with an electron gas density parameter, $r_s = 2.07a_0$, appropriate for aluminium. The potential $V_0(z; F_{ext})$ is calculated self-consistently, in the density functional scheme [24] as applied by Schreier and Rebentrost [25], using the boundary condition that the electric field F should be uniform and equal to $2F_{ext}$ far from the surface. The details of the approximation for the exchange–correlation part of the potential are given at the end of this subsection. For the sample, $V_s(z) = V_0(z; F_{ext})$ gives rise to a repulsive and confining potential, while for the tip, $V_t(z) = V_0(z; -F_{ext})$ gives rise to a barrier that the electrons can tunnel through. The interface potential is now obtained by matching $V_s(z)$ and $V_t(z)$ at a point z_m in the linear asymptotic region as

$$V_i(z) = \begin{cases} V_s(z) & z < z_m \\ V_t(s - z) + V + \Phi_t - \Phi_s & z > z_m \end{cases} \tag{2.1}$$

where Φ_s and Φ_t are the work functions of the substrate and tip, respectively, V is the bias, and the tip–sample distance s, measured relative to the jellium edges of the tip and sample respectively, is determined by the condition that $V_i(z)$ should be continuous at z_m. This matching gives rise to an implicit relation between the distance s, the field F and the bias V. In the particular experimental set-up, the tip is made of Ir that has a work function ~1.5 eV larger than Al, but it is very likely that it is covered by Al atoms [26]. As a consequence, the contact potential in the experiments may vary between 0 and 1.5 eV. In the discussions, we will use the lower limit as an example, corresponding to an Al tip, but we will, when comparing to experiments, also present results that account for the maximum work function difference of 1.5 eV, corresponding to an Ir tip. This is done by choosing $\Phi_t - \Phi_s = 1.5$ eV in equation (2.1) [27]. We will see that the important issue is to have a good model of the substrate. A typical interface potential shape obtained as in equation (2.1), with $\Phi_s = \Phi_t$, is shown in figure 1. Note that we have an extended linear part in the interface potential due to the relatively low bias $V = 4.0$ eV and large tip–surface separation $s = 17$ Å. The electric field $F = 0.20$ eV Å^{-1}, is close to what is expected from an assumption based on an extended region of a uniform electric field between the tip and the sample, $V/s = 0.24$ eV Å^{-1}.

In order to model the (static) image barrier effects, it is necessary to include the long-range image potential of a metal surface. We proceed as proposed by Serena and coworkers [28] as follows. The local density approximation (LDA) for the exchange–correlation potential V_{xc} is used in the bulk and up to the location of the image plane. Beyond that, a non-local form for the potential is used, of the form

$$V_{xc}^{nl}(z) = -\frac{1 - [1 + b(z - z_{ip})/4]\, e^{-b(z - z_{ip})}}{4(z - z_{ip})} \tag{2.2}$$

where z_{ip} is the location of the image plane and b is a parameter chosen to give the LDA value for V_{xc}^{nl} at z_{ip}. The location of the image plane is also calculated self-consistently in that the position of the centroid of the excess charge, due to the applied external field,

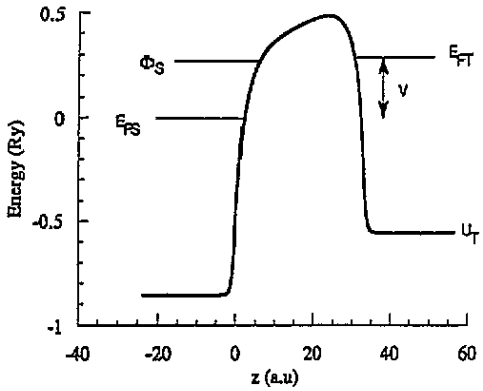

Figure 1. Model of sample tip potential, where the sample is to the left and the tip is to the right. Both tip and sample are represented by a semi-infinite jellium with $r_s = 2.07$ corresponding to aluminium. An external field F is applied ($+F$ on the sample and $-F$ on the tip), mimicking the effect of the applied bias voltage. The difference in Fermi energies of tip and substrate $E_{FT} - E_{FS}$ is equal to the bias voltage V. The two self-consistent solutions for a semi-infinite jellium in the presence of $\pm F$ are matched at their respective linear part which here is around 15 au from the jellium edge of the substrate ($z = 0$). The substrate work function Φ_s (defined for $F = 0$) and the tip band bottom U_t are also indicated.

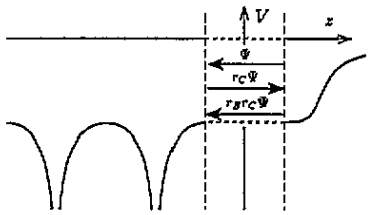

Figure 2. Schematic multiple-scattering geometry. An incident wave Ψ with unit flux towards the crystal is partly reflected at a reference plane. Its reflected part is given by $r_c\Psi$ where r_c is the (complex) crystal reflectivity. This part is reflected at the barrier reference plane which has a reflectivity r_b. The multiply scattered parts are summed to give the total wave Ψ_{tot}.

is taken as z_{ip} at *every* iteration. When self-consistency is reached, the value of z_{ip} is stable. This approach yields values for z_{ip} that are essentially the same as Lang and Kohn's calculated values using linear response of a jellium to a test charge [29]. If exchange effects are important, there will be a modification to the results from this treatment [30]. As demonstrated by Eguiluz *et al* [30], a 'Kohn–Sham' electron 'feels' an image plane location closer to the surface than a test charge does ($z_0 = 0.72$ au instead of 1.46 au for $r_s = 2.07$). These effects are even more pronounced for larger r_s values.

2.2. *Inclusion of sample ion cores*

The scattering of the electrons from the Al sample ion cores is handled perturbatively using pseudopotential theory. We confine ourselves to the situation where we are in an energy range far from band gaps. Such a situation, and the fact that Al can be represented by a weak pseudopotential, suggest a treatment of the scattering of the electrons from the ion cores using the Born approximation. The detailed derivation of the reflectivity, r_c, in this approximation is presented in the appendix, where we also discuss the connection between our approach and the standard two-band model. The resulting Born expression for the reflectivity of a semi-infinite crystal measured relative to the first lattice plane (see figure 2) is given by

$$r_c(k', k) = -i\frac{v(k' - k)}{|a \times b|\,|k_z|\,(1 - e^{i(k-k')\cdot c})}. \tag{2.3}$$

Here k and k' are the wavevectors of the incident and scattered wave, respectively, $v(k'-k)$ is the form factor, i.e. the Fourier transform of the atomic pseudopotential, a and b are the surface basis vectors, and c connects an atom to a neighbouring atom in the next atomic layer further into the crystal. In the case of Al(111), the area of the surface unit cell is given by $|a \times b| = \sqrt{3}a^2/4$ and the distance [31] d between crystal planes parallel to the surface is $d = a/\sqrt{3}$, where $a = 7.7$ au is the bulk lattice constant of Al. The surface periodicity gives the restriction $k'_{\parallel} = k_{\parallel} + g_{\parallel}$, where $g_{\parallel}$ is a surface reciprocal lattice vector. There is no such restriction for the momentum transfer perpendicular to the surface. Note that the result for r_c in equation (2.3) neglects possible modifications of the form factor for the atoms in the surface region and also neglects the possibility of (geometrical) surface relaxation [32]. Furthermore, the behaviour of the denominator with momentum transfer explicitly shows that this expression breaks down when the transfer comes close to a Brillouin zone boundary where a band gap opens up.

In order to estimate the reflectivity, we have chosen a pseudopotential form factor which was originally fitted to the measured phonon dispersion of bulk aluminium [33]. The justification for the use of such a pseudopotential is that we are sufficiently close in energy to the Fermi level. This pseudopotential reproduces accurately the width of the band gap in the (111) direction located about 5 eV below ϵ_F [34]. In the tunnelling situation we find that the effective tunnelling occurs from states with perpendicular energy close to the Fermi level, i.e., $k_{\parallel} \sim 0$. Considering then specular reflection of an electron propagating normal to the surface, $k_{\parallel} = k'_{\parallel} = 0$ and $-k_z = k'_z = k$, the pseudopotential form factor does not vary much for energies around the vacuum level $\epsilon - \epsilon_F \sim 4$ eV, where $2k/k_F \approx 2.3$. For this situation, we have from equation (2.3) that,

$$|r_c| = \frac{|v(2k)|}{2|a \times b|\,|\sin(kd)|} \qquad \phi_c = \pi. \tag{2.4}$$

Here, and in the following, the phase shift ϕ_c is taken with respect to the jellium edge z_0 and includes thus an extra phase due to the electron motion between the first crystal layer and the jellium edge. In previous analyses [14, 22], ϕ_c was erroneously evaluated as $\sim 4\pi$, which has consequences on the energy of the resonances but not on their existence. The value of $|r_c|$ is around 0.1 as obtained from (2.4), while the actual value of ϕ_c is determined from the sign of $v(2k)/\sin(kd)$; $v(2k)$ is positive and $\sin(kd)$ is negative in the described situation. The value $|r_c| = 0.1$ will be used throughout in our calculations. Finally, we would like to stress, as shown in the appendix, that a simple two-band model underestimates $|r_c|$ in an energy region far away from a band gap.

The range of applicability of the result in equation (2.3) is not restricted to aluminium but can be applied to other free-electron-like materials. The condition that has to be fulfilled in order for the Born expression to be valid is that we apply it in an energy range sufficiently far from projected band gaps. However, if the effect of the crystal reflectivity is to be noticeable, we need a reflectivity comparable to the one for aluminium. We find similar and even larger reflectivities e.g for Pb and Ba. In the case of Pb, there is a band gap with a width of ~ 3 eV at 3.5 eV below the Fermi energy, so it may be out of the range of the application of the Born approximation. In the case of Ba(100), we have equally favourable conditions as in the case of Al(111) so there is a chance to experimentally resolve 'crystal-derived' image resonances on that surface.

2.3. *Tunnelling current*

We describe in the following the calculation of the tunnelling current and the conductance in our interface potential and show how the effects of the sample ion cores can be accounted

for in these calculations by using the calculated crystal reflectivity r_c.

The tunnelling current density J_0 for two free-electron systems in a planar geometry is given by the expression [35]

$$J_0 = \frac{1}{2\pi^2}\left[\int_{\epsilon_{FT}-V}^{\epsilon_{FT}} d\epsilon_z\ (\epsilon_{FT}-\epsilon_z)|T_0(\epsilon_z)|^2 + V\int_{U_t}^{\epsilon_{FT}-V} d\epsilon_z\ |T_0(\epsilon_z)|^2\right] \tag{2.5}$$

where V is the bias, $T_0(\epsilon_z)$ is the transmission amplitude of electrons through the barrier with an energy, ϵ_z, normal to the surface. Further, $\epsilon_{FT} = \epsilon_{FS} + V$ and ϵ_{FS} are the Fermi energies of the tip and the sample, respectively, and U_t is the energy of the tip band bottom. All energies are measured relative to the vacuum level, $\epsilon_{vac} = \epsilon_{FS} + \Phi_s$, of the field-free sample, where Φ_s is the work function of the sample. The first term gives the contribution to J_0 from tip electrons tunnelling into unoccupied states of the sample and the second term the net contribution to J_0 from tip and sample electrons tunnelling between occupied states. Before we show how the effects of the crystal potential influence the tunnelling current, we will first show that, in the situation of interest, the dominant contribution to J_0 comes from electrons with ϵ_z within a few tenths of an eV from ϵ_{FT} ($k_\parallel \sim 0$). In particular the contribution from the second term in (2.5) to J_0 is negligible.

The transmission amplitude, $T_0(\epsilon_z)$, has been determined from the electron wavefunctions in $V_t(z)$ by a direct numerical integration of the one-electron Schrödinger equation based on a modified midpoint method and Richardson extrapolation [37]. The boundary conditions in a potential like that in figure 1 for electron wave functions through the barrier are

$$\Psi(z) = \begin{cases} e^{-ik_1 z} + r(\epsilon_z)\,e^{ik_1 z} & \text{for } z \to \infty \\ t(\epsilon_z)\,e^{-ik_2 z} & \text{for } z \to -\infty \end{cases} \tag{2.6}$$

where $r(\epsilon_z)$ is the amplitude of the reflected wave on the tip side and $t(\epsilon_z)$ the amplitude of the transmitted wave on the substrate side. We have that the momentum $k_1 = \sqrt{2(\epsilon_z - U_t)}$ and $k_2 = \sqrt{2(\epsilon_z - U_s)}$ where U_s is the energy of the substrate band bottom. The transmission coefficient is then given by $|T_0(\epsilon_z)|^2 = (k_2/k_1)|t|^2$.

At the tip–sample distances, s, and biases, V, appropriate for the scanning tunnelling experiment, we obtain typically very small transmission probabilities for the tip electrons. For instance, under the conditions prevailing in figure 1, we find that $|T_0(\epsilon_{FT})|^2 \sim 10^{-9}$. Such a small $|T_0(\epsilon_{FT})|^2$ suggests that the magnitude can be understood from a single-bounce WKB approximation for the penetration of the electron wave through the barrier. In this approximation, the transmission probability through the barrier is given by

$$|T_0^{WKB}(\epsilon_z)|^2 \sim e^{-W} \tag{2.7}$$

where

$$W = 2\int_{z_1}^{z_2} \sqrt{2(V(z)-\epsilon_z)}\,dz \tag{2.8}$$

and z_1 and z_2 are the classical turning points in the tip–sample interface potential $V_t(z)$ of an electron with energy ϵ_z normal to the surface. The behaviour of W can be understood from a trapezoidal model for the barrier potential, which gives

$$W = \begin{cases} (4\sqrt{2}/3F)(\Phi_t^{3/2} - (\Phi_s - V)^{3/2}) & V < \Phi_s \\ (4\sqrt{2}/3F)\Phi_t^{3/2} & V > \Phi_s \end{cases} \tag{2.9}$$

where Φ_t is the workfunction of the tip. In the (field emission) region $V > \Phi_s$, the tunnelling distance, $s_t \equiv z_2 - z_1$, varies with F, while in the region $V < \Phi_s$, s_t is constant

and equal to the tip–sample distance s. An estimate of the magnitude of the transmission probability based on (2.7)–(2.9) with $\Phi_t = \Phi_s$ and for conditions as in figure 1 gives $|T_0^{WKB}(\epsilon_{FT})|^2 \sim 10^{-10}$ which is about the same magnitude as the calculated value.

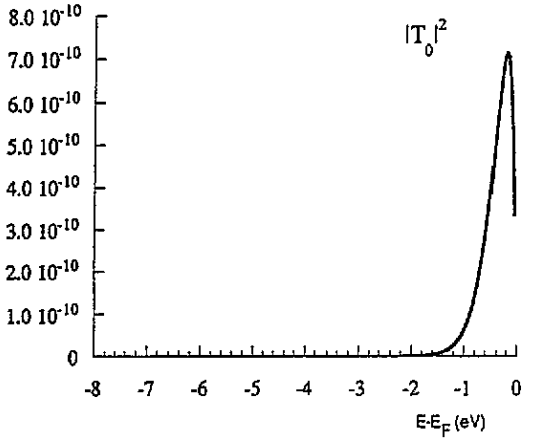

Figure 3. Energy variation of the calculated transmission coefficient for an Al 'tip'. The bottom of the band is at −11.7 eV.

The WKB result in (2.7) and (2.8) shows also directly that $|T_0(\epsilon_z)|^2$ will increase rapidly with ϵ_z due to a decreasing magnitude of the negative kinetic energy in the barrier. A Taylor expansion in ϵ around ϵ_{FT} of the action integral in (2.8) gives

$$|T_0^{WKB}(\epsilon_z)|^2 \sim |T_0^{WKB}(\epsilon_{FT})|^2 e^{-(\epsilon_{FT}-\epsilon_z)/\Delta} \tag{2.10}$$

where

$$\Delta = \left(2\int_{z_t}^{z_2} \frac{dz}{\sqrt{2(V(z)-\epsilon_{FT})}}\right)^{-1}. \tag{2.11}$$

An application once again of the trapezoidal model to $V_i(z)$ gives the estimate

$$\frac{1}{\Delta} \sim \begin{cases} (4/\sqrt{2}F)(\Phi_t^{1/2} - (\Phi_s - V)^{1/2}) & V < \Phi_s \\ (4/\sqrt{2}F)\Phi_t^{1/2} & V > \Phi_s. \end{cases} \tag{2.12}$$

Under the conditions in figure 1, we find from the estimate in (2.12) a small value for Δ, about 0.1 eV, due to a large $s_t \approx 17$ Å, which suggests that the tunnelling is dominated by electrons in states with ϵ_z close to ϵ_{FT}. Correspondingly, $k_\parallel$ is close to zero. The prefactor $\epsilon_{FT} - \epsilon_z$ in the first term of (2.5) vanishes exactly at the Fermi level due to the vanishing density of states at $\epsilon_z = \epsilon_{FT}$ which makes the tunnelling dominated by states with $\epsilon_z \approx \epsilon_{FT} - \Delta$. The calculated $(\epsilon_{FT} - \epsilon_z)|T_0(\epsilon_z)|^2$, shown in figure 3, clearly demonstrates a behaviour of rapid exponential decrease with decreasing ϵ_z over just a few tenths of an eV. We estimate Δ as 0.15–0.2 eV. Hence, the second term in (2.5) is negligible and the first term can accurately be represented by the approximation

$$J_0 \approx \frac{e\Delta^2}{2\pi^2}|T_0(\epsilon_{FT} - \Delta)|^2 \tag{2.13}$$

where Δ is now obtained from the exponential decrease of the calculated $|T_0(\epsilon_z)|^2$. In practice, we have already shown that Δ is so small that it can be ignored in the argument of the transmission coefficient in (2.13). Furthermore, the results from the simple trapezoidal model, equation (2.12), shows that Δ will not be exponentially dependent on s, like the transmission probability, and can be assumed to be constant in the calculation of J_0.

We demonstrate further how the effects of the sample ion cores modify the tunnelling current. In principle, we need to calculate the current carried by the Bloch wave propagating into the sample. This is done here by noting that, from particle conservation, this current is given by $1 - |r_c|^2$ times the current of the wave incident on the crystal. The multiple scattering of the electron wave between the crystal potential and the barrier potential (see figure 2) results in an amplification of the wave incident on the crystal with the factor $1/(1 - r_b r_c)$. Hence, the transmission coefficient in this situation is simply obtained by multiplying $|T_0|^2$ with

$$R_{\text{tunn}}(\epsilon) = \frac{1 - |r_c|^2}{|1 - r_b r_c|^2} \tag{2.14}$$

where r_b is the reflection amplitude of an incoming wave from the sample on the barrier.

The final result for the tunnelling current density J that we use in our calculations is obtained by collecting the results in (2.13) and (2.14) and is given by

$$J \approx \frac{\Delta_0^2}{2\pi^2} R_{\text{tunn}}(\epsilon_{\text{FS}} + V)|T_0(\epsilon_{\text{FS}} + V)|^2 \tag{2.15}$$

where Δ_0^2 is assumed to be constant and Δ is neglected in the argument of the transmission coefficient. The current density J in (2.15) depends on two independent control parameters—the tip–sample distance s and the bias V—through the interface potential and the argument $\epsilon_{\text{FS}} + V$.

Scanning tunnelling experiments often record the conductance versus bias, $(\mathrm{d}I/\mathrm{d}V)$–$V$, in a constant-current mode, i.e., the bias is varied under the condition that the current is constant. Since we are only able to calculate current densities in our planar model, we make a comparison between the observed $(\mathrm{d}I/I\,\mathrm{d}V)$–$V$ in a constant-current mode and the calculated $(\mathrm{d}J/J\,\mathrm{d}V)$–$V$ in a constant-current-density mode. The latter quantity has been calculated in the following way: (i) for initial V and J which fixes F and s, $\mathrm{d}J/\mathrm{d}V$ is calculated using (2.15), upon a small change of V by δV; (ii) V is increased and F and s are adjusted so that J across the new barrier is the same within 3% of the original J; (iii) $\mathrm{d}J/\mathrm{d}V$ is then calculated as in (i) for this new V. A smaller tolerance than 3% in the current gives no change in the resulting curves and the functional dependence of $V_i(z)$ on F is obtained by an interpolation between potentials calculated for a set of different fields.

2.4. Surface density of states

Since we are in a regime where the dominant contribution to the tunnelling comes from states with ϵ_z close to $\epsilon_{\text{FT}} = \epsilon_{\text{FS}} + V$, we attempt to relate $\mathrm{d}J/J\,\mathrm{d}V$ to a surface DOS of the sample in the presence of a positive external uniform field. In order to do that, we need first to define the surface DOS for electrons with $k_\parallel = 0$ and show how it is influenced by the crystal reflectivity.

In a situation where we are concerned with the scattering of electrons that are incident normal to the crystal, the propagation is described by a one-dimensional potential, $V_s(z)$. The surface density of states $n_s(\epsilon)$ of the surface region, $z > z_0$, is then defined as an integral over the local DOS,

$$n_s(\epsilon) \equiv \int_{z_0}^{\infty} \rho(z;\epsilon)\,\mathrm{d}z \tag{2.16}$$

where the local DOS, $\rho(z;\epsilon)$, is determined from the retarded Green function, $g(z, z';\epsilon)$, of $V_s(z)$ as

$$\rho(z;\epsilon) = -\frac{1}{\pi}\mathrm{Im}\; g(z, z;\epsilon). \tag{2.17}$$

Note that we have explicitly excluded the spin degeneracy in (2.16). We evaluate $\rho(z;\epsilon)$ in (2.17) using a standard representation of the Green function [36] and we arrive at:

$$\rho(z;\epsilon) = R(\epsilon)\rho_0(z;\epsilon) \tag{2.18}$$

where

$$R(\epsilon) = \frac{1-|r_c|^2}{1+|r_c|^2-2|r_c|\cos(\phi)} \tag{2.19}$$

and $\phi = \phi_b + \phi_c$. Note that $R(\epsilon)$ is independent of z. Here $\rho_0(z;\epsilon)$ is the local DOS when $r_c = 0$ and is given by

$$\rho_0(z;\epsilon) = \frac{1}{2\pi k}|\psi_>(z)|^2 \tag{2.20}$$

where $\psi_>(z)$ is the wave function on the barrier side. Similar expressions for $\rho(z;\epsilon)$ have also been given by Radny [38] using a semiclassical approach. In the evaluation of the integral in (2.16) over $\rho(z;\epsilon)$, we use a method introduced by Echenique and Pendry [1, 9] which is based on introducing an infinitesimal absorption in the Schrödinger equation. An application of this method to the integral over $|\psi_>(z)|^2$ gives

$$\frac{1}{k}\int_{z_0}^{\infty} dz|\psi_>(z)|^2 = \frac{d\phi_b}{d\epsilon}(\epsilon) + \frac{\sin\phi_b(\epsilon)}{2\epsilon}. \tag{2.21}$$

The term $(\sin\phi_b)/2\epsilon$ comes from the interference between the incident and scattered wave from the barrier [39] and is dependent on the position of z_0. Using the result in (2.21) and the definition (2.16) of $n_s(\epsilon)$ we obtain, in the absence of a crystal reflectivity, $r_c = 0$,

$$n_s^0(\epsilon) = \frac{1}{2\pi}\left[\frac{d\phi_b}{d\epsilon}(\epsilon) + \frac{\sin\phi_b(\epsilon)}{2\epsilon}\right] \tag{2.22}$$

and in the situation of a non-zero crystal reflectivity,

$$n_s(\epsilon) = R(\epsilon)n_s^0(\epsilon). \tag{2.23}$$

Hence, *all* the effects of the crystal reflectivity both on surface and local DOS are just included in $R(\epsilon)$ as defined in (2.18). Note that we have a similar result for the effects on the transmission coefficient in (2.14) through the factor $R_{tunn}(\epsilon)$. This factor differs only from $R(\epsilon)$ by the fact that r_b is defined in (2.14) for $V_i(z)$ while in (2.19) it is defined for $V_s(z)$. The differences between r_b are very small in these two situations since the transmission coefficient is very low through $V_i(z)$.

In the calculations of $n_s(\epsilon)$ and $n_s^0(\epsilon)$, the barrier phase shift, ϕ_b, and its energy derivative are obtained from the wavefunctions calculated numerically from the one-electron Schrödinger equation in $V_s(z)$. The magnitude of the crystal reflectivity $|r_c|$ and its phase shift, ϕ_c, have been extracted from equation (2.4).

3. Results and discussion

We begin by presenting tunnelling spectra, $dJ/J\,dV$ calculated in a constant-current-density mode in the tip–sample interface potential. These spectra are then related to the surface electronic structure of the sample potential in the presence of a static external field by examining the calculated surface density of states, $n_s(\epsilon)$, for electrons with $k_{\parallel} = 0$. In particular, we study the effects of the crystal reflectivity on the tunnelling spectra and compare to the surface density of states. Finally, we make a direct comparison of the calculated tunnelling spectra with experimental data.

3.1. Calculated tunnelling spectra

The most important point of our work is the peak at V below Φ_s in the calculated $(dJ/J\,dV)$–V curves, as shown in figure 4, which is present *only* when the effects of the crystal reflectivity are included. This peak has a completely different origin from the oscillatory structure for biases V larger than Φ_s. It is a 'crystal-derived' barrier resonance formed by a reflection back and forth of the electron wave from the crystal and the barrier. The precise position in V of this resonance below Φ_s is dependent on the behaviour of ϕ_c and ϕ_b.

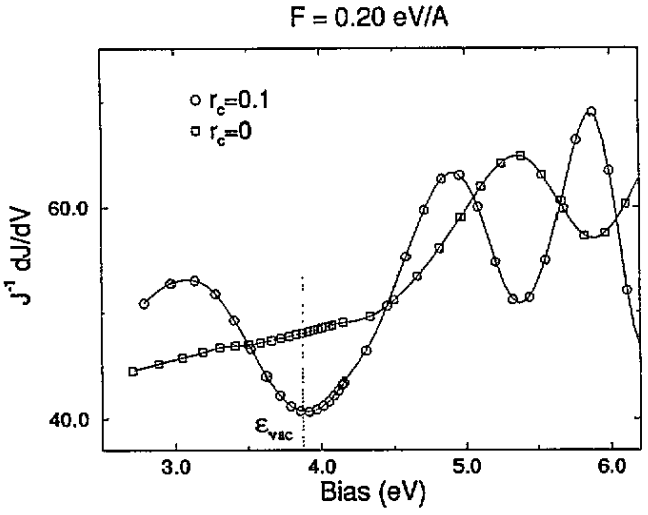

Figure 4. Tunnelling curves, $(dJ/J\,dV)$—V, for a system of an Ir tip and an Al(111) substrate for an initial field strength of 0.20 eV Å, with and without inclusion of the crystal pseudopotential. It is only when the crystal reflectivity is taken into account that we get a conductance peak below the metal vacuum level (3.87 eV). The lines connecting the calculated points are cubic spline interpolations.

The oscillatory structure in the calculated $(dJ/J\,dV)$–V curve for $V > \Phi_s$ is, as shown, present independent of crystal effects of the sample. This kind of oscillation has been previously identified both in scanning tunnelling experiments [5, 6] and in theoretical models similar to our model [7, 21, 40]. The issue of the characterization of this oscillatory structure in terms of 'field-induced' resonances has been brought up earlier [5, 6, 7, 21] with different viewpoints. Binnig *et al* [5] and García *et al* [21], interpreted all peaks as being a Stark-shifted Rydberg series, whereas Becker and coworkers [6] presented their results as standing waves formed between the probe and the sample, as Gundlach resonances [41], having nothing to do with surface electronic states. We will come back to the nature of these oscillations in the discussion of field effects on surface DOS.

In order to justify the approximation (2.15) that we use in the calculation of $(dJ/J\,dV)$–V curves, we examine the calculated curves more closely. In figure 4, the constant J mode corresponds to having a constant $|T(\epsilon_{FT})|^2$. At the lowest bias of $V = 2.8$ eV, we have $|T(\epsilon_{FT})|^2 = 10^{-7}$ and $s = 15$ Å. While keeping $|T(\epsilon_{FT})|^2$ constant with varying V ($2.8 < V < 6.8$ eV), s increases from 15 to 42 Å and F increases (in an oscillatory manner) from 0.17 to 0.21 eV Å. This behaviour is in line with what is expected from the WKB treatment of the trapezoidal model introduced in section 2.1: according to (2.7), $|T(\epsilon_{FT})|^2$ is governed by the tunnelling distance s_t when $V > \Phi_s$ and s has to increase almost linearly with V in order to keep s_t constant. This variation of s with V also makes F stay more or less constant. The largest variation of F in our calculations occurs accordingly at low biases, while it varies much more slowly for $V > \Phi_s$. More importantly, this behaviour of s_t and F with V in the constant-J mode is consistent with the approximation of keeping Δ constant according to the WKB-result in (2.12) which is a crucial test of our approximation.

Moreover the effects on J due to the broadening and shift from $\Delta \approx 0.2$ eV which is neglected in (2.15) is much smaller than the energy scale for the structures in the calculated $(\mathrm{d}J/J\,\mathrm{d}V)$–$V$ curve which are $\sim$1 eV.

Our approximate expression for the current density in (2.15) is thus well justified and shows that J reveals the sample electronic structure at an energy $\epsilon_{FS} + V$. The reflection coefficient from the barrier part of $V_t(z)$ at the energy $\epsilon_{FS} + V$ will be very close to the corresponding coefficient for $V_s(z)$ with the same F. We can then relate the $(\mathrm{d}J/J\,\mathrm{d}V)$–$V$ curves directly to the surface DOS, of $V_s(z)$ at a fixed F.

3.2. *Calculated Surface DOS*

There is a clear one to one correspondence between the peaks in the calculated $(\mathrm{d}J/J\,\mathrm{d}V)$–$V$ curves in figure 4 and $n_s(\epsilon)$ of $V_s(z)$, as calculated at fixed F, in figure 5. When the lattice effects are switched on, a 'crystal-derived' peak occurs below the vacuum level and the peaks above the vacuum level narrow and shift slightly to lower energies. The oscillatory structure due to the 'field-induced' resonances is also present at energies above $\epsilon_{FS} + \Phi_s$. This fact shows that the tunnelling spectra curves can be understood in terms of the density of states of the surface where the tip has been replaced by an external field. We begin by discussing the image resonances in $n_s(\epsilon)$ for zero external field and end by a discussion of how these resonances are modified in the presence of an external field. In particular we will show that the 'crystal-derived' barrier resonance in $n_s(\epsilon)$ comes from the multiple scattering between the crystal and the surface barrier.

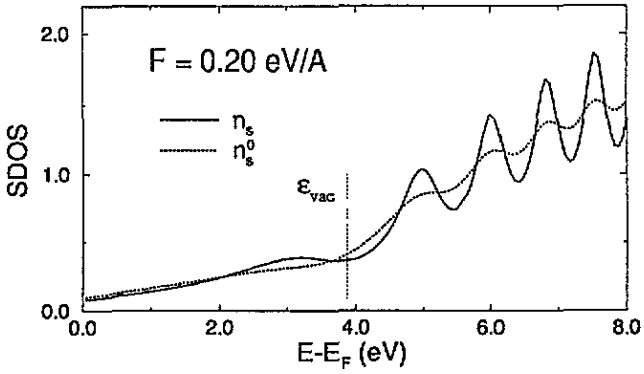

Figure 5. Surface density of states of the Al(111) sample in the presence of an external field $F = 0.2$ eV Å. The field strength, F is kept constant for all energies. In $n_s(\epsilon)$, the reflectivity from the sample ion cores is included, $|r_c| = 0.1$, while in $n_s^0(\epsilon)$ we have $|r_c| = 0$.

3.2.1. Analysis of the field-free case: $F = 0$. The effect of the scattering between the crystal and the surface barrier on $n_s(\epsilon)$ is described by the prefactor, $R(\epsilon)$, in (2.23). The spectral features of $n_s(\epsilon)$ are directly understood from the behaviour of $R(\epsilon)$. At values of $|r_c|$ well below 0.5 like in our case where we are far from a band gap, $R(\epsilon)$ is well approximated by only including a single scattering event from the crystal,

$$R(\epsilon) \approx 1 + 2|r_c| \cos \phi(\epsilon) \tag{3.1}$$

where the weak energy dependence of $|r_c|$ has been ignored. In this situation, $R(\epsilon)$ and thus $n_s(\epsilon)$ will show an oscillatory behaviour with a series of maxima at energies ϵ_m determined by a phase condition corresponding to constructive interference as

$$\phi(\epsilon_m) \equiv \phi_b(\epsilon_m) + \phi_c(\epsilon_m) = 2\pi m \tag{3.2}$$

where m is an integer. The well known divergence of ϕ_b for an image barrier at the vacuum level results in a Rydberg series of maxima with decreasing separation, converging to ϵ_{vac} [11]. Using an appropriate WKB approximation for ϕ_b for an image potential [11], and the phase condition in (3.2), a Rydberg series is obtained as

$$\epsilon_m = \epsilon_{vac} - \frac{1}{32(m+a)^2}. \tag{3.3}$$

Here the energy variation of ϕ_c has been neglected and $a = \frac{1}{2}(1 - \phi_c/\pi)$. The phase shift in the Born approximation, $\phi_c = \pi$, gives that the lowest member in the image series lies at -0.85 eV below ϵ_{vac}, which is close to ~ -1 eV that we obtain in our surface barrier model. This difference can be understood from the fact that the image plane position z_{ip} in our model lies at $\sim 1.5a_0$ instead of $z_{ip} = 0$, which gives rise to a larger barrier phase shift ϕ_b. Finally, we note that in a situation where $|r_c|$ is close to one [42] e.g. close to a band gap, the maxima of $R(\epsilon)$ turn into narrow Lorentzian resonance peaks at the same energies ϵ_m.

3.2.2. Effects of an external field: $F \neq 0$. In figure 6, the energies of the SDOS resonances of Al(111) are shown as a function of field strength. When turning on the electric field F, $V_s(z)$ increases in the surface region which in turn, gives an overall decrease and convergence of ϕ_b to a finite value at ϵ_{vac} since the classical turning point of the barrier potential is finite for all ϵ. This effect limits the number of members in the image series below $\epsilon_{FS} + \Phi_s$, i.e. the vacuum level for $F = 0$, and shift up their energies with increasing F. This fact is demonstrated by figure 6 where there exists only *one* barrier resonance even down to field strengths as low as 0.05 eV Å. This resonance is by us referred to as a 'crystal-derived' barrier resonance since it disappears when the reflectivity from the crystal is switched off as shown in figure 5. The members of the image series which shift up above $\epsilon_{FS} + \Phi_s$ for finite F have changed their character into 'field-induced' resonances since their energy position will now be determined by the contribution to ϕ_b from the linear part of the potential.

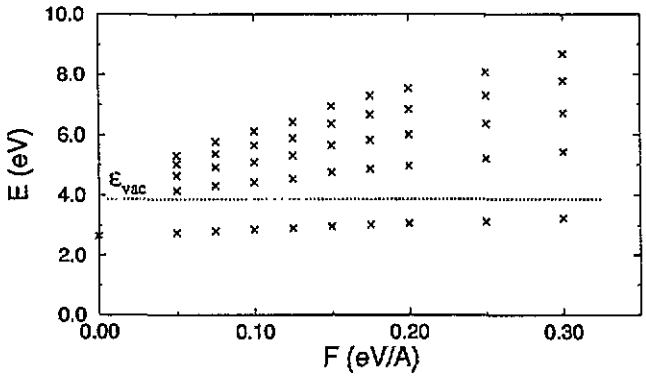

Figure 6. Energies of the resonances in the surface density of states of Al(111) as a function of the applied (static) field strength. The energy position of the 'crystal-derived' (image) resonance for the field-free case is also indicated.

In contrast to the 'crystal-derived' barrier resonance or the image resonances, it is not necessary for the existence of 'field-induced' resonances that there is a non-zero reflectivity from the crystal. The sharp variation in the surface barrier potential, when going from bulk to the linear region of the $V_s(z)$, is sufficiently rapid, compared to the wavelength of the electron, to give rise to a non-zero reflectivity of an electron wave incident on this part of barrier from the linear region of $V_s(z)$. Such a behaviour cannot be understood in the WKB approximation as stressed, e.g., by Gundlach [41].

We can make a closer analysis of the behaviour of the 'field-induced' resonances by finding a similar $\tilde{R}(\epsilon)$ to $R(\epsilon)$ that describes these resonances. Such a factor can be found from equation (2.19) simply by changing the location of z_0 to a position $\tilde{z}_0$ in the linear region of $V_s(z)$ whereby r_c and r_b are modified to $\tilde{r}_c$ and $\tilde{r}_b$. The reflectivity, $\tilde{r}_c$, includes now also the reflectivity of the electron waves from the rapid variation of $V_s(z)$ around the jellium edge of the sample, earlier included in r_b. The result in (2.18) is also valid in this situation and the local DOS can be expressed as

$$\rho(z;\epsilon) = \tilde{R}(\epsilon)\tilde{\rho}_0(z;\epsilon) \tag{3.4}$$

where $\tilde{\rho}_0(z;\epsilon)$ is determined as in (2.20) from a wave function $\tilde{\psi}_>(z) \propto \psi_>(z)$ but with an incident amplitude of unity at $z = \tilde{z}_0$ on the barrier. All the 'field-induced' resonances in $n_s(\epsilon)$ will now be described by $\tilde{R}(\epsilon)$. The calculated $n_s^0(\epsilon)$ in figure 5 shows that we do not have any narrow resonances whose width is much less than the level separation. Hence, also in this case we have a small value for $|\tilde{r}_c|$ due to the reflection of $V_s(z)$ at the selvedge and the lineshape is given by an oscillatory function like in (3.1). A small value for $|\tilde{r}_c|$ in this situation is consistent with the observation that the inclusion of the crystal reflectivity makes the amplitudes of the 'field-induced' resonances increase by more than a factor of two. The non-linear variation of the 'field-induced' resonance energies with F as shown in figure 6 can be understood from the behaviour of $\tilde{\phi}_b$ with respect to F. We evaluate the WKB approximation for $\tilde{\phi}_b$ in a linear repulsive potential $V_s(\tilde{z}_0) + F(z - \tilde{z}_0)$. The resulting approximate phase shift is then given by

$$\tilde{\phi}_b(\epsilon) \approx \frac{4\sqrt{2}}{3}\frac{\epsilon^{3/2}}{F} - \frac{\pi}{2}. \tag{3.5}$$

If the energy variation of $\tilde{\phi}_c$ is neglected, we obtain directly from (3.2) the approximate resonance energies (relative to $V_s(\tilde{z}_0)$),

$$\epsilon_m \approx \left(\frac{3\pi}{\sqrt{8}}\right)^{2/3} F^{2/3}(m + \tfrac{1}{4} + \alpha)^{2/3} \tag{3.6}$$

where α is determined from $\tilde{\phi}_c$. For instance, in the case of a triangular well with an infinite potential barrier at $z = \tilde{z}_0$, α is equal to $-\frac{1}{2}$. The non-linear power law behaviour of ϵ_m with F in (3.6) with an exponent less than one fits the calculated variation of the 'field-induced' resonances in figure 6. Best agreement is obtained for the high-lying resonances.

3.3. Comparison with experiments

The prime objective with the comparison of the results from our one-dimensional potential model with the measured tunnelling spectra on Al(111) is to show that one of the observed peaks in the measured spectra originates from the 'crystal-derived' barrier resonance of the sample potential. Since the work function of the Ir tip is unknown due to its likely covering by Al atoms, we will discuss the experimental data in relation to results both from an Ir and an Al tip model.

The experimental tunnelling spectra are recorded in a constant-current mode under different initial tunnelling gap distances, corresponding to several values of the tunnelling current. The relative change in distance with bias is known experimentally, but the initial gap distance cannot be determined. Spectra for current values in the range 4–102 pA are shown in figure 7. Two peaks are clearly discernible in all spectra and at the lowest tunnelling current even a third peak can be resolved at higher biases. An increase of the bias from 4 to 7 eV at $I \sim 100$ pA corresponds to an increase of about 14 Å [26]. This

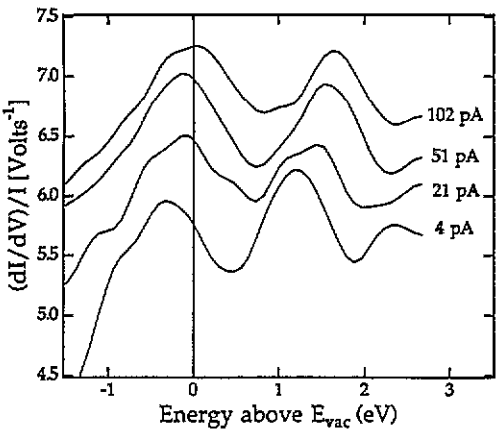

Figure 7. Experimental differential conductance curves for tunnelling currents of 4–102 pA, recorded in a constant-current mode.

observation in the field emission region of the tunnelling suggests that the field strength is about 0.2 eV Å. In figure 8, we have consequently presented results of $(dJ/J\,dV)$–V in the Ir tip model for a set of initial field strengths, 0.20, 0.25, and 0.30 eV Å, and for the Al tip model for a field strength of 0.20 eV Å. Note that there are no differences in the peak positions for the two models [43].

The calculated and measured tunnelling spectra agree in important ways. The observed peak separations in the measured $(dI/I\,dV)$–V are well reproduced by the narrow range of field strengths of 0.2 to 0.25 eV Å in the calculated $(dJ/J\,dV)$–V. The calculated data reproduce also nicely the observed shift of the peak positions to higher V with increasing I, corresponding to higher J in the calculations. The shift of the peak positions to higher V with increasing I is understood in our model from the fact that an increase of J at a fixed V corresponds to a decrease in the tunnelling distance and an increase of F. Such an increase of F will shift up the resonance positions in $n_s(\epsilon)$ as shown in figure 6 with a concomitant increase of the positions of the corresponding peaks in the tunnelling spectra.

As demonstrated in our discussion of figure 4, the first peak in the calculated tunnelling spectra with a position below Φ_s is a 'crystal-derived' barrier resonance and the higher lying peaks derive from 'field-induced' resonances of the sample potential. The fact that there is an observed peak *below* the vacuum level leads us to the interpretation that it is a 'crystal-derived' barrier resonance while the other peaks, well above the vacuum level, are due to 'field-induced' resonances. The observed position of the 'crystal-derived' peak in figure 7 seems to occur at a bias ~0.5 V higher than the calculated peak position [44]. However, in the calculations of the tunnelling spectra, we have neglected the fact that the effective tunnelling occurs $\Delta \sim 0.2$ eV below ϵ_{FT} (see equation (2.11)). Accounting for that would shift the calculated peak position up in bias with Δ, yielding better agreement with experiment. Moreover, we would like to stress that the peak position is sensitive to the model potential used. Thus, further work on the improvement of the model potential both in the surface region and for the crystal would be of great interest.

In this context, we would like to comment on the relevance of dynamical effects of the tunnelling through the potential barrier on the peak positions in the tunnelling spectra. There have been some model studies on the dynamical effects of the image potential on the tunnelling through a potential barrier relevant for STM [45]. These studies have shown that there is a reduction of the contribution of the image potential to the interface potential if the 'traversal' time for tunnelling τ is smaller than the inverse surface plasmon frequency ω_{sp}^{-1}, i.e., if $\tau\omega_{sp} < 1$. If this regime applied in our case, a static image potential approximation would then give a too low potential barrier with the implication that the calculated peak

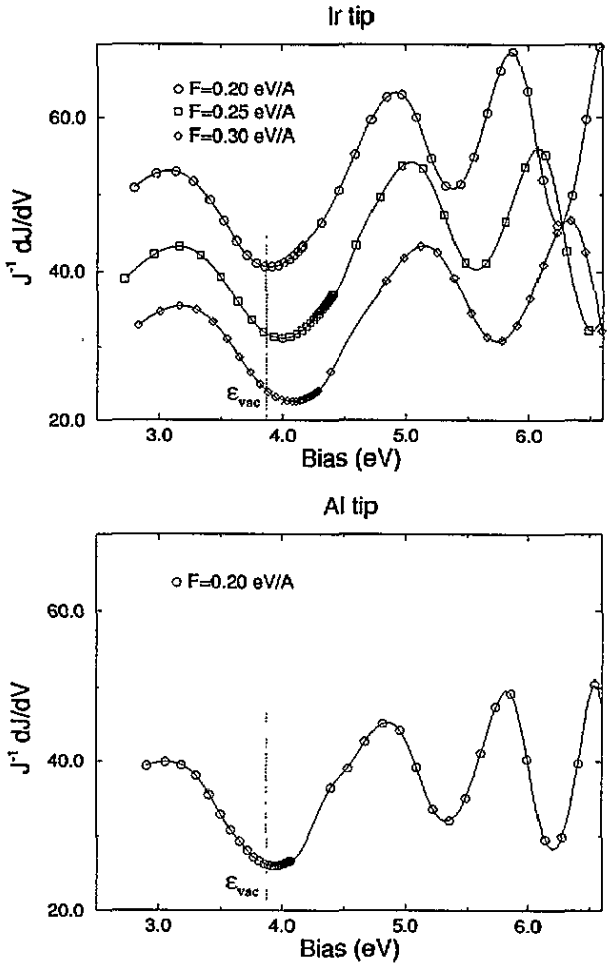

Figure 8. Calculated conductance $((1/J)\mathrm{d}J/\mathrm{d}V)$ curves for different initial field strengths, corresponding to different tunnel currents, for an Ir tip and an Al tip. The indicated field strengths F apply only to the first point in each curve; the requirement of constant tunnel current throughout the calculations makes the field strength vary slightly with bias V. The lines between the points in the curves are spline interpolations and serve primarily as guides to the eye.

positions would appear at a lower bias in the tunnelling spectra than in a calculation based on a dynamic image potential. However, we find that for the relevant tunnelling conditions a static approximation of the image barrier potential is well justified in our model. This is based on the WKB result for the 'traversal' time [46], $\tau = 1/2\Delta$, and the fact that Δ is $\sim$0.2 eV which makes $\omega_{sp}\tau = \omega_{sp}/2\Delta \approx 25$ for Al where $\omega_{sp} \sim 10$ eV. Dynamic effects are thus unlikely to have a major influence on the image potential here.

4. Summary

We have extended a previously developed model [14] for formation of electronic resonances on free-electron-like surfaces to include static external fields, thus enabling us to compare with scanning tunnelling spectroscopy (STS) data from such surfaces [22]. This model is appropriate for application on free-electron-like surfaces at energies sufficiently far from band gaps. The crystal reflectivities obtained in our approach and from the often used two-band model are compared and it is found that the two-band model underestimates seriously the reflectivity of the crystal at energies far from the band gap considered.

We demonstrate that a peak in the calculated conductance curves of Al(111), below the

vacuum level in a region with no projected band gaps, is a 'crystal-derived' image resonance introduced by the image potential and the weak scattering from the Al crystal lattice. The observed peak in the STS spectra below the vacuum level is therefore attributed to this resonance. Moreover, we argue that the precise position of this peak is a sensitive test of the surface barrier and the crystal potential. We believe that such resonances influence the IPE spectra through the surface density of states and thus that IPE features can be interpreted in such terms and not only in terms of matrix element effects as suggested earlier [16].

Acknowledgments

This work has been supported by the Swedish Natural Science Research Council (NFR) and in part by the USA's National Science Foundation under grants DMR 91-03466 and DMR 94-07055. Discusssions with Bob Bartynski are gratefully acknowledged.

Appendix. Derivation of the reflectivity of a semi-infinite crystal

A1. Born approximation

The scattering from a semi-infinite crystal of a nearly-free-electron metal may be described by a weak potential V_c, and a treatment based on the first-order Born approximation which is justified at energies far away from any band gap. We derive the result for the reflectivity from a semi-infinite crystal using a local V_c, but the derivation can also be done for a non-local and energy-dependent pseudopotential.

The first-order Born approximation is based on the approximation of replacing the total wave in the integrand of the Lippman–Schwinger equation by the incoming wave as

$$\Psi^{\text{Born}}(r) = \Psi_{\text{in}}(r) + \frac{2m}{\hbar^2}\int \mathrm{d}^3r'\, G_0(r-r')V_c(r')\Psi_{\text{in}}(r') \tag{A1}$$

where $\Psi^{\text{Born}}(r)$ is the total wave, $\Psi_{\text{in}}(r) = \mathrm{e}^{\mathrm{i}k_i r}$ is the incident wave with $k_{iz} < 0$ with the crystal side on $z < 0$. The two-dimensional scattering geometry makes it convenient to use a wavevector expansion parallel to the surface of the retarded free-particle Green function given by

$$G_0(r-r') = -\frac{\mathrm{i}}{2}\int \frac{\mathrm{d}^2k_\parallel}{(2\pi)^2}\frac{\mathrm{e}^{\mathrm{i}k_z|z-z'|}\,\mathrm{e}^{\mathrm{i}k_\parallel\cdot(r_\parallel - r'_\parallel)}}{k_z} \tag{A2}$$

where k_z and $k_\parallel$ denote the momentum components perpendicular and parallel to the surface, respectively. For the propagating waves, we have $k_\parallel < k_i$ and $k_z = \sqrt{k_i^2 - k_\parallel^2}$ while for the evanescent waves $k_\parallel > k_i$ and $k_z = \mathrm{i}\sqrt{k_\parallel^2 - k_i^2}$.

The crystal potential, $V_c(r)$, in (A1) is now expressed as a sum over atomic potentials, $v(r)$, located at atomic sites r_n as

$$V_c(r) = \sum_n v(r - r_n). \tag{A3}$$

After inserting this sum into (A1) and using the wavevector representation in (A2), the sum over n factorizes into an atomic form factor and a structure factor as

$$\sum_n \int \mathrm{d}^3r'\, v(r'-r_n)\,\mathrm{e}^{\mathrm{i}(k_i-k)\cdot r'} = v(k-k_i)\sum_n \mathrm{e}^{\mathrm{i}(k_i-k)\cdot r_n}. \tag{A4}$$

By making use of the translational symmetry of the semi-infinite system of atoms with one atom in each unit cell, the structure factor in (A4) can now be expressed as

$$\sum_n e^{i(k_i-k)\cdot r_n} = \frac{4\pi^2}{|a\times b|}\sum_{g_\parallel}\delta((k_{i\parallel}-k_\parallel)-g_\parallel)\frac{1}{1-e^{i(k_i-k)\cdot c}} \tag{A5}$$

where a and b are surface base vectors for atoms within an atomic layer parallel to the surface, c is a vector connecting an atom to another neighbouring atom in the next atomic layer further into the crystal, and $g_\parallel$ is a reciprocal surface lattice vector. The delta functions in (A5) reduce the scattered wave, Ψ_{scatt}, outside the crystal to a sum over outgoing plane waves with wavevectors k_f satisfying the two-dimensional Bragg condition that $k_{f\parallel}-k_{i\parallel}=g_\parallel$ and we obtain the result

$$\Psi_{scatt}(r)=\sum_{g_\parallel} f\left(k_f=k_{i\parallel}+g_\parallel+\sqrt{k_i^2-(k_{i\parallel}+g_\parallel)^2}\hat{z},k_i\right)e^{ik_f\cdot r} \tag{A6}$$

where the scattering amplitude $f(k_f,k_i)$ (or r_c) is given by

$$f(k_f,k_i)=-\frac{im}{\hbar^2}\frac{1}{|a\times b|}\frac{v(k_f-k_i)}{|k_{iz}|(1-e^{i(k_i-k_f)\cdot c})}. \tag{A7}$$

Note that there is a sign error in the exponent in equation (3), corresponding to the expression in (A7), of our previous work [14]. In the more general situation for non-local potentials, where we still can express the crystal potential as a lattice sum over the atomic potentials as in (A3), the derivation still goes through with $v(k_f-k_i)$ replaced by $\langle k_f|v|k_i\rangle$ in (A7).

A2. Connection between the two-band model and the Born approximation

We will here show how the reflectivity obtained in a two-band model as e.g. applied by Radny to Al [15] is related to the result in the Born approximation. In particular, we will demonstrate that a two-band model can seriously underestimate the reflectivity outside a band gap. We will consider a situation most appropriate for the tunnelling experiment, normal incidence and specular scattering, corresponding to the restriction $k_\parallel=0$ and $k'_\parallel=0$ for the incident and scattered wave, respectively.

In a two-band model the Schrödinger equation for an electron in an infinite crystal is solved in the basis of two plane waves, e^{-ik_bz} and $e^{-i(k_b-g)z}$,

$$\Psi_b(z)=a\,e^{-ik_bz}+b\,e^{-i(k_b-g)z} \tag{A8}$$

where g is a reciprocal lattice vector normal to the surface. We will be primarily concerned with the case of $g=2\pi/d$ where d is the perpendicular distance between the atomic planes. The amplitudes a and b and the electron energy ϵ are determined from an eigenvalue problem as

$$\frac{b}{a}=\frac{2V_g}{2\epsilon-(k_b-g)^2} \tag{A9}$$

and

$$\epsilon=\frac{k_b^2}{2}+\frac{2\,|\,V_g\,|^2}{2\epsilon-(k_b-g)^2} \tag{A10}$$

where V_g is the Fourier component of the crystal potential corresponding to the wave vector g. In particular, at the zone boundary, $k_b=g/2$, a band gap opens up with a width $2|V_g|$ at the energy $\epsilon_g\equiv(g/2)^2/2$.

The reflectivity, r_c, of the semi-infinite crystal is now obtained by matching, at the surface ($z=0$), an incident and reflected plane wave in free space, $\Psi(z)=e^{-ikz}+$

$r_c e^{ikz}$, $z > 0$, to the two-band solution $\Psi_b(z)$. In this work we are only concerned with the case where the energy is far away from the band gap, $|\epsilon - \epsilon_g| \gg 2|V_g|$ where $k_b \simeq k$. In this limit, r_c is small and proportional to the amplitude of the wave $e^{-i(k_b-g)z}$ in the crystal ($r_c \simeq (b/a)(g/(2k))$),

$$r_c \simeq \frac{1}{\mathcal{V}} \frac{v(g)}{k(2k-g)} \tag{A11}$$

where V_g has been expressed in terms of $v(g)$ and the volume, $\mathcal{V}$, of the primitive cell, $\mathcal{V} = |a \times b|d$. Using the same value for $V_g \approx 0.24$ eV as Radny [15] for $g = 2\pi(1, 1, 1)/a$ of the Al(111) surface, we obtain a reflectivity amplitude of only about 1.1% at an energy close to the vacuum level, to be compared to the about 10 times larger amplitude obtained in the Born approximation. Note that the pseudopotential form factor [33], as used in the Born approximation, reproduces correctly this value for V_g which agrees with the measured band gap.

In order to understand the origin of the different magnitudes of r_c, we make a comparison of the reflectivity obtained in the two-band model with the result in (A7) from the Born approximation. According to (A7), the Born approximation for the reflectivity is given by

$$r_c^{\text{Born}} = -i\frac{1}{|a \times b|} \frac{v(2k)}{k} \frac{1}{1 - e^{i2kd}}. \tag{A12}$$

This result reduces to the result in the two-band model if the following two conditions are fulfilled: (i) $|k - g/2| \ll g/2$ and (ii) $v(2k) \approx v(g)$. Condition (i) allows a Taylor expansion of the exponential function in equation (A12) around $k = g/2$ which simplifies r_c to

$$r_c^{\text{Born}} \simeq \frac{1}{\mathcal{V}} \frac{v(2k)}{k(2k-g)}. \tag{A13}$$

The only difference between the results in the Born approximation and the two-band model, equations (A13) and (A11), respectively, is that in the former case the atomic form factor is probed at the actual momentum transfer, while in the latter case the argument for the form factor is fixed at a momentum transfer corresponding to the reciprocal lattice vector g. Hence the two results agree if the condition (ii) is also fulfilled.

The prime reason for the breakdown of the two-band model for describing r_c close to the vacuum level of Al(111) is that the condition (ii) is violated. $v(2k)$ is about a factor of six larger than $v(g)$ at the relevant range of k [33] ($k \approx 3g/4$), which accounts for most of the discrepancy between the reults for r_c in the two-band model and the Born approximation. Moreover, the restriction of the two-band model to include only two plane waves is simply not justified to describe weak scattering far away from band gaps. This can be understood from the fact, that when including additional plane waves from higher-order reciprocal lattice vectors in equation (A8), the corresponding contributions to r_c will be of the form given in equation (A11) for energies far away from band gaps. However, these additional contributions can be sizable since each one decays slowly away from the band gap introduced by the corresponding vector g. The primary aim of the two-band model is rather to describe the opposite situation of strong scattering close to a band gap.

References

[1] Echenique P M and Pendry J B 1978 *J. Phys. C: Solid State Phys.* **11** 2065
[2] McRae E G 1979 *Rev. Mod. Phys.* **51** 541
[3] Jones R O, Jennings P J and Jepsen O 1984 *Phys. Rev.* B **29** 6474
[4] Nordlander P and Tully J C 1989 *Surf. Sci.* **211/212** 207

[5] Binnig G, Frank K H, Fuchs H, Garcia N, Reihl B, Rohrer H, Salvan F and Williams A R 1985 *Phys. Rev. Lett.* **55** 991
[6] Becker R S, Golovchenko J A and Swartzentruber B S 1985 *Phys. Rev. Lett.* **55** 987
[7] Pitarke J M, Flores F and Echenique P M 1990 *Surf. Sci.* **234** 1
[8] Garcia R 1990 *Phys. Rev.* B **42** 5479
[9] Echenique P M and Pendry J B 1990 *Prog. Surf. Sci.* **32** 111
[10] Weinert M, Hulbert S L and Johnson P D 1985 *Phys. Rev. Lett.* **55** 2055
Himpsel F J 1986 *Comment. Condens. Matter Phys.* **12** 199
Pendry J B, Larsson C G and Echenique P M 1986 *Surf. Sci.* **166** 57
Kubiak G D 1988 *Surf. Sci.* **201** L475
[11] Smith N V 1985 *Phys. Rev.* B **32** 3549
[12] Heskett D, Frank K-H, Koch E E and Freund H-J 1987 *Phys. Rev.* B **36** 1276
Heskett D, Frank K-H, Horn K, Koch E E, Freund H-J, Baddorf A, Tsuei K-D and Plummer E W 1988 *Phys. Rev.* B **37** 10387
[13] Lindgren S A and Walldén L 1989 *Phys. Rev.* B **40** 11546
[14] Papadia S, Persson M and Salmi L-A 1990 *Phys. Rev.* B **41** 10237
[15] Radny M 1990 *Surf. Sci.* **231** 43
[16] Schaich W L and Lee J T 1991 *Phys. Rev.* B **44** 5973
Schaich W L 1992 *Phys. Rev.* B **45** 3744
[17] Baratoff A 1984 *Physica* B **127** 143
[18] Lang N D 1986 *Phys. Rev.* B **34** 5947
[19] Selloni A, Carnevali P, Tosatti E and Chen C D 1985 *Phys. Rev.* B **31** 2602
[20] Feenstra R M, Stroscio J A and Fein A P 1987 *Surf. Sci* **181** 295
[21] García R, Sáenz J J, Soler J M and García N 1987 *Surf. Sci.* **181** 69
[22] Yang S, Bartynski R A, Kochanski G P, Papadia S, Fondén T and Persson M 1992 *Phys Rev. Lett.* **70** 849
[23] Lang N D 1992 *Phys. Rev.* B **45** 13599
[24] Kohn W and Sham L J 1965 *Phys. Rev* **140** A1133
[25] Schreier F and Rebentrost F 1987 *J. Phys. C: Solid State Phys.* **20** 2609
[26] Kochanski G P 1992 private communication
[27] Note that the potential used for the tip always corresponds to a semi-infinite jellium with $r_s = 2.07a_0$.
[28] Serena P A, Soler J M and Garcia N 1986 *Phys. Rev.* B **34** 6767
[29] Lang N D and Kohn W 1973 *Phys. Rev.* B **7** 354
[30] Eguiluz A G and Hanke W 1989 *Phys. Rev.* B **39** 10433
Eguiluz A G, Heinrichsmeier M, Fleszar A and Hanke W 1992 *Phys. Rev. Lett.* **68** 1359
[31] In the relevant situations, we are concerned with normal incidence and scattering. In this case c is replaced with its normal component—the distance between layers d.
[32] The measured surface relaxation of Al(111) in
Nielsen H B and Adams D L 1982 *J. Phys. C: Solid State Phys.* **15** 615
has been found to be only about 1% between the first and second layer and can be neglected.
[33] Wallace D C 1969 *Phys. Rev.* **187** 991
[34] Levinson H J, Greuter F and Plummer E W 1983 *Phys. Rev.* B **27** 727
[35] Duke C B 1969 *Tunnelling in Solids (Solid State Physics Supplement 10)* (New York: Academic)
[36] Arfken G 1985 *Mathematical Methods for Physicists* 3rd edn (London: Academic)
[37] Press W H, Flannery B P, Teukolsky S A and Vetterling W T 1986 *Numerical Recipes—The Art of Scientific Computing* (Cambridge: Cambridge University Press)
[38] Radny M 1991 *J. Phys. C: Solid State Phys.* **3** 5525
[39] It is important to also put $k \to k + i\delta$ in the flux normalization of Echenique and Pendry, which seems to be omitted in their analysis; otherwise, the second term in (2.21) will not be obtained.
[40] Bono J and Good R H 1987 *Surf. Sci.* **188** 153
[41] Gundlach K H 1966 *Solid-State Electron.* **9** 949
[42] Note that r_c can be calculated in many ways. In the Born approximation, it is not meaningful to assign values for $|r_c|$ close to one, whereas it is fully justifiable in other approaches.
[43] The positions of the peaks in the calculated tunnelling spectra are insensitive to our modelling of the work function of the tip as can be seen from the comparison of the calculated tunnelling spectra in figure 8 for the Ir and Al tip where $\Phi_t - \Phi_s = 1.5$ eV and $\Phi_t = \Phi_s$, respectively. This effect can be understood from the fact that the resonance positions are determined by the interface potential on the sample side which is not very much influenced by the presence of the tip in our situation of small transmission probabilities. The prime effect of the Ir tip is that there will be a contact potential difference of about 1.5 eV between

the tip and the sample even at zero bias. This difference makes the tunnelling distances larger for the Ir tip at the same F and V than for the Al tip with no contact potential difference.

[44] Note that the value of Φ_s in the jellium model is about 0.4 eV lower than the measured Φ of Al(111) We compensate for that by making the comparison of the peak positions with respect to $V - \Phi_s$ instead of V in figure 7.

[45] Michalewicz M T and Mahanty J 1986 *Phys. Lett.* **116A** 392
Persson B N J and Baratoff A 1988 *Phys. Rev.* B **38** 9619

[46] Büttiker M and Landauer R 1982 *Phys. Rev. Lett.* **49** 1739